*Journal of Applied Mechanics and Technical Physics, Vol. 48, No. 1, pp. 71–79, 2007*

# SOME FEATURES OF THE FLOW AROUND RAPIDLY ROTATING BODIES MADE OF CELLULAR-POROUS MATERIALS

**V. K. Baev, A. V. Fedorov, V. M. Fomin, and T. A. Khmel'**

UDC 532.546

*Two types of gas flows arising near a rapidly rotating cellular-porous disk are studied numerically and experimentally. Steady-state limits for the flow around a disk rotating in free space and the type and scenario of the loss of stability are determined. Transitional flows are characterized by formation of a vortex sheet at the boundary of the exhausting jet. Numerical simulations of the flow around a cellular-porous disk rotating near a flat screen show that it is possible to form a closed swirl flow responsible for redistribution of swirl in the gap between the disk and the flat screen. The computed results offer an explanation for the experimentally observed excess of tangential velocity of the flow in the gap over the velocity of disk rotation.*

**Key words:** *cellular-porous materials, rotation, internal and external flows, experiment, numerical simulation.*

**Introduction.** The prospects of application of highly permeable cellular-porous materials (CPM) in fabricating rotors of multifunctional energy-conversion devices [1] imply the necessity of studying gas-flow parameters inside and outside rapidly rotating bodies made of such materials. External and internal aerodynamics inherent in rotation of CPM bodies was studied theoretically and experimentally in [2, 3]. A mathematical model within the framework of mechanics of heterogeneous media was developed in [2], and a technique for computing axisymmetric spatial swirl flows inside and outside rotating CPM bodies was developed and tested in [3]. The steady-state flow near a body rotating with a constant velocity is determined by a time-dependent method in solving unsteady equations of the mathematical model. Numerical computations are performed in a domain including both the porous body and some part of the ambient space. It was shown [3] that numerical solutions for the flow inside and in the vicinity of a porous body computed in a large closed domain coincide with solutions computed in a comparatively moderate-size domain with appropriate "soft" conditions on the input and output boundaries. The latter case requires a shorter computer time. After determining the wave flow field near the rotating body, verification of the mathematical model used was performed. The computed momentum and dynamic pressure were found to be in good agreement with the measured results.

The present work, which is a continuation of [2, 3], contains new numerical and experimental data, which reveal the specific features of the flow in the vicinity of rotating CPM bodies in space bounded by the screen and in unbounded space. The mechanism of instability leading to development of low-frequency oscillations of the flow and the possibility of swirl redistribution in the flow between the rotating CPM disk and the flat screen are analyzed.

**Stability of the Flow Around a Rotating Body Made of a Cellular-Porous Material (Problem 1).** Gas flows inside and outside a rapidly rotating cellular-porous body was numerically simulated in [3]. For Reynolds numbers corresponding to the test conditions (diameter of the CPM disk equal to 150 mm and velocity of rotation equal to 2000–5000 rpm), the steady-state solution was found to exist and to be uniquely determined by a time-dependent method for different initial conditions, including zero initial conditions (quiescent gas). Persistence of

Khristianovich Institute of Theoretical and Applied Mechanics, Siberian Division, Russian Academy of Sciences, Novosibirsk 630090; fedorov@itam.nsc.ru; khmel@itam.nsc.ru. Translated from Prikladnaya Mekhanika i Tekhnicheskaya Fizika, Vol. 48, No. 1, pp. 86–96, January–February, 2007. Original article submitted February 27, 2006.

the steady-state solution in an unsteady problem and convergence to this solution from different initial data confirm that the solution is stable to small and finite axisymmetric perturbations. In some particular cases, the internal flow can be determined by solving the corresponding boundary-value problem for a system of ordinary differential equations. A comparison of numerical solutions with solutions of a system of ordinary differential equations shows that the numerical solution converges to the unique solution as the grid step is decreased.

In model problems solved to test the numerical algorithm, the domain boundaries were subjected to no-slip conditions or conditions of symmetry, i.e., the effect of boundary layers was actually ignored. Under these conditions, the real (or artificial) viscosity of the medium exerted only a stabilizing effect on the solution, because it was relatively small. In computing the flow around a real model of a porous disk soldered to an impermeable solid substrate [3], boundary-layer formation was taken into account in imposing the boundary conditions for tangential velocity. The characteristics of the corresponding unique steady flow (dynamic pressure and moment of rotating forces) agree with experimental data.

It was also noted in experiments that low-frequency and low-amplitude oscillations of the flow arise in some cases. A possible reason for their emergence is the loss of stability of the steady flow. Flow stability is analyzed below by the method of direct numerical simulation for the case with an increasing Reynolds number, which corresponds to an increase in rotation velocity of the disk with fixed geometric parameters under the test conditions. The objective of the present work was to determine the range of Reynolds numbers where the flow remains steady and to analyze the evolution of unsteady perturbations and the character of transitional flows.

We consider a cylindrical body made of a porous-cellular material, which is located in free space and is set into motion around its axis with a certain angular velocity. A forced flow caused by centrifugal convection is formed inside the body during its rotation. Within the framework of the model considered in [2], the incompressible gas flow inside and outside the body is described by vorticity and stream function equations [3]:

$$\frac{\partial\chi}{\partial t}-\frac{1}{r}\frac{D(\chi,\psi)}{D(r,z)}=-\frac{1}{r^2}\frac{\partial}{\partial z}w^2-\frac{1}{r}\Big(\frac{\partial f_z}{\partial r}-\frac{\partial f_r}{\partial z}\Big)+\frac{1}{r^2\,\mathrm{Re}}\Big[r\frac{\partial}{\partial r}\Big(\frac{1}{r}\frac{\partial\,(r^2\chi)}{\partial r}\Big)+\frac{\partial^2\,(r^2\chi)}{\partial z^2}\Big],$$

$$\frac{\partial\,(rw)}{\partial t}-\frac{1}{r}\frac{D(rw,\psi)}{D(r,z)}=-rf_\theta+\frac{1}{\mathrm{Re}}\Big[r\frac{\partial}{\partial r}\Big(\frac{1}{r}\frac{\partial\,(rw)}{\partial r}\Big)+\frac{\partial^2\,(rw)}{\partial z^2}\Big], \tag{1}$$

$$r^2\chi=\frac{\partial^2\psi}{\partial r^2}-\frac{1}{r}\frac{\partial\psi}{\partial r}+\frac{\partial^2\psi}{\partial z^2},\qquad \frac{D(\chi,\psi)}{D(r,z)}=\frac{\partial\chi}{\partial r}\frac{\partial\psi}{\partial z}-\frac{\partial\psi}{\partial r}\frac{\partial\chi}{\partial z},$$

$$u=-\frac{1}{r}\frac{\partial\psi}{\partial z},\qquad v=\frac{1}{r}\frac{\partial\psi}{\partial r},\qquad \chi=\frac{1}{r}\Big(\frac{\partial v}{\partial r}-\frac{\partial u}{\partial z}\Big).$$

Here $r$, $z$, and $\theta$ are the cylindrical coordinates, $u$, $v$, and $w$ are the radial, longitudinal, and tangential components of velocity, $\boldsymbol{f}$ is the volume force vector, $\chi$ is the modified vorticity, and $\psi$ is the stream function. The characteristic scales of the problem are the angular velocity of rotation $\Omega$, the radius of the porous cylinder $R$, the characteristic velocity $R\Omega$, the gas density $\rho_0$, the time scale $1/\Omega$, and the Reynolds number $\mathrm{Re}=R^2\Omega/\nu$ ($\nu$ is the kinematic viscosity). In the general case, the dimensionless force of interaction between the gas and the porous skeleton is $\boldsymbol{f}=K|\boldsymbol{v}-r\boldsymbol{i}_\theta|(\boldsymbol{v}-r\boldsymbol{i}_\theta)+L(\boldsymbol{v}-r\boldsymbol{i}_\theta)$. The dimensional parameters of body drag $k=K/R$ and $\lambda=L\Omega$ depend on material properties, porosity of the structure, and gas viscosity [4]. The external flow is also described by system (1) with $\boldsymbol{f}=0$.

The steady flow is described by Eqs. (1) and by the boundary conditions

$$\begin{aligned}
&r=0\text{:}\quad && \psi=0,\quad w=0,\quad \chi=0,\\
&z=0\text{:}\quad && \frac{\partial\psi(r,z)}{\partial z}=0,\quad \chi(r,0)=0,\quad w(r,0)=0,\\
&r=r_1\text{:}\quad && \frac{\partial^2\psi(r,z)}{\partial r^2}=0,\quad \frac{\partial^2\chi(r,z)}{\partial r^2}=0,\quad \frac{\partial^2 w(r,z)}{\partial r^2}=0\quad\text{at}\quad u(r_1,z)>0,\\
&&& \frac{\partial^2\psi(r,z)}{\partial r^2}=0,\quad \chi(r,z)=0,\quad w(r,z)=0\quad\text{at}\quad u(r_1,z)\leqslant 0,\\
&z=z_0\text{:}\quad && \psi=0,\quad \frac{\partial w}{\partial z}=0,\quad \frac{\partial\chi}{\partial z}=0.
\end{aligned} \tag{2}$$

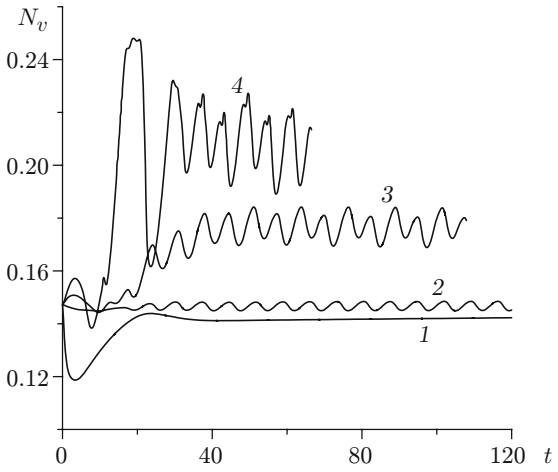


Fig. 1. Time evolution of the functional $N_v$ for $\mathrm{Re} = 10^4$ (1), $6.5 \cdot 10^4$ (2), $10^5$ (3), and $6.4 \cdot 10^5$ (4).

To solve problem (1), (2), we used Arakawa's explicit finite-difference scheme, Libman's iterative method, and the procedure of nested averaging [5–7]. The computational domain is determined as $0 \leqslant r \leqslant r_1$, $0 \leqslant z \leqslant z_1$, where the porous body occupies the region $0 \leqslant r \leqslant 1$, $z_1 - z_0 \leqslant z \leqslant z_1$, with $\boldsymbol{f} = 0$ outside this region.

The computations were performed with the following parameters: $K = 1$, $L = 0$, $r_1 = 3$, $z_1 = 2$, and $z_0 = 0.5$.

Similar to [3], the integral characteristic whose behavior can indicate solution convergence is the numerical functional

$$N_v = \Delta_r \Delta_z \sum_i^{N_r} \sum_j^{N_z} 0.5(u_{ij}^2 + v_{ij}^2 + w_{ij}^2) r_i.$$

Figure 1 shows the time evolution of $N_v$ with a varied Reynolds number. It is seen that the steady-state solution is reached at $\mathrm{Re} \leqslant 10^4$, whereas this characteristic periodically oscillates at $\mathrm{Re} \geqslant 6.5 \cdot 10^4$. With increasing Reynolds number, not only an increase in amplitude of oscillations but also its modulation is observed, i.e., oscillations of higher frequencies are imposed onto the basic oscillations, though the frequency of the latter remains almost unchanged.

An analysis of local characteristics of the flow for this problem allows us to obtain the dynamic pattern of instability evolution. Figure 2 shows the flow patterns in the plane $(r, z)$ for $\mathrm{Re} = 3.2 \cdot 10^5$ with a time step equal to 1.08. The streamlines are plotted in Fig. 2a (the porous body is shown as a rectangle), and the fields of modified vorticity are shown in Fig. 2b. As in [3], the gas enters the porous cylindrical body through the end face $z = 1.5$, $0 < r < 1$ and partly through the outer side surface $1.5 < z < 2$, $r = 1$. Gas ejection from the porous body into the ambient space through the remaining part of the side surface occurs owing to centrifugal convection forces in the form of a jet directed along the plane of symmetry $z = 2$. The jet also possesses a certain swirl. The modified vorticity $\chi$ acquires the maximum values at the jet boundary (Fig. 2b).

It follows from Fig. 2a that a closed circulation flow is formed on the jet boundary in the vicinity of the corner of the porous body, near the side surface. The vortex character of this flow can also be seen in Fig. 2b. The vortex is shifted along the jet with time and is entrained from the flow field. Obviously, the vortex appears with a certain period (cf. streamlines 1 and 7, 2 and 8 in Fig. 2a) approximately equal to 6.5 and, correspondingly, with a frequency several times lower than the frequency of rotation of the body. Regular formation and entrainment of such vortices is responsible for periodic changes in both local and integral characteristics of the flow, which is manifested in the behavior of the function $N_v(t)$ (see Fig. 1). A further increase in the Reynolds number leads to origination of subharmonics (secondary instability) and subsequent chaotization of the flow. Such a behavior is consistent with the theory of transition to turbulence through a sequence of bifurcations [8].

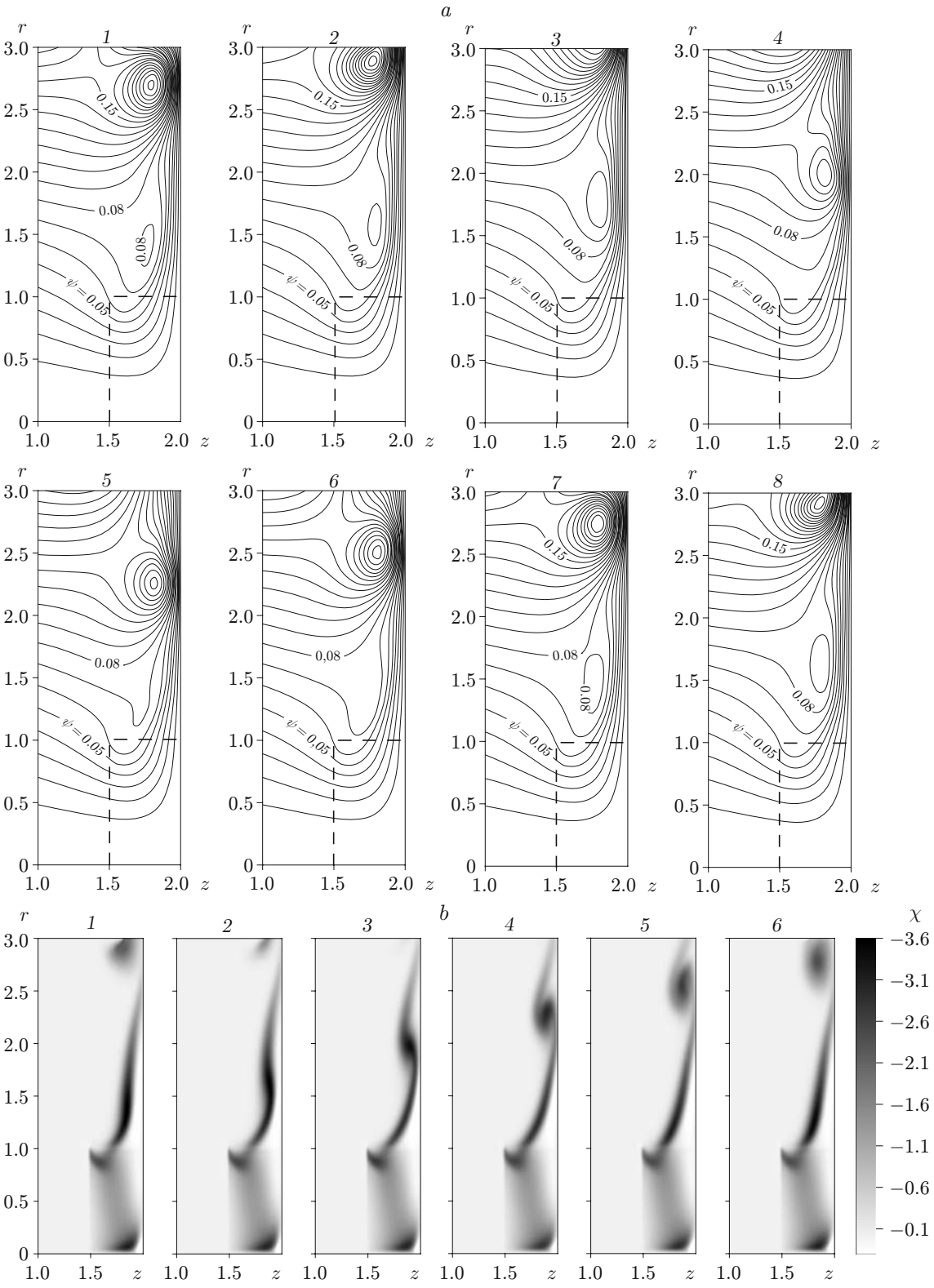


Fig. 2. Periodic flow around a porous disk rotating with a constant velocity ($\mathrm{Re} = 3.2 \cdot 10^5$ and $\Delta t = 1.08$): (a) streamlines; (b) modified vorticity.

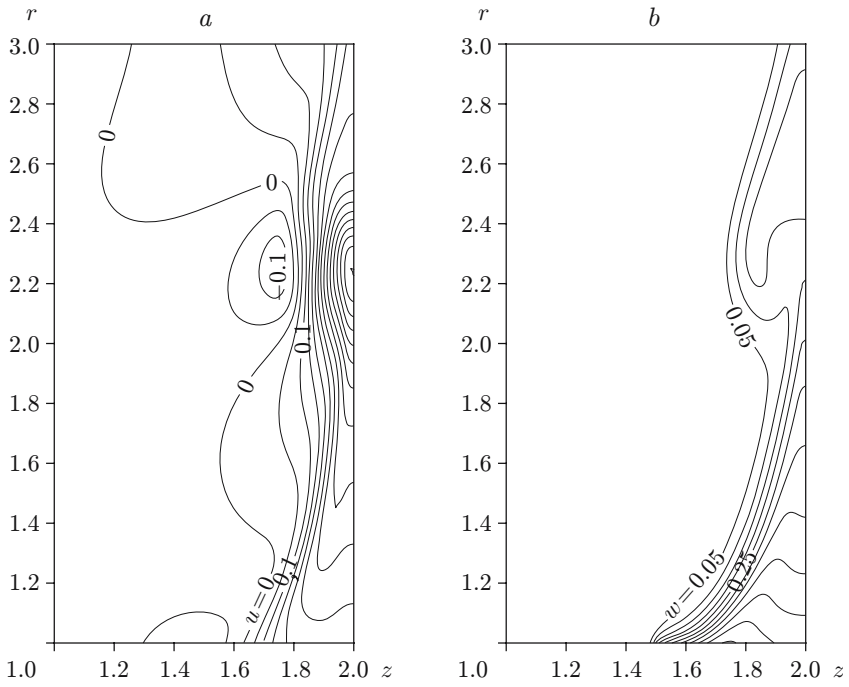


Fig. 3. Typical shape of the jet exhausting from a rotating porous disk: (a) isolines of radial velocity $u$; (b) isolines of tangential velocity $w$.

To determine the nature of the primary instability, we analyze the flow near the boundary of the jet ejected with high velocity from a porous body into a weak external flow. This boundary is presented as concentration of lines in Fig. 3, which shows the isolines of the radial and tangential components of velocity corresponding to the pattern of isolines 1 in Fig. 2a. The profiles of these parameters in the direction perpendicular to the boundary have a deflection point. Thus, origination of vortices is, apparently, caused by instability of the Kelvin–Helmholtz type [8].

The spatial trajectories of an element of the fluid volume in the vortices being formed are helical lines, because rotational motion in the azimuthal direction in the plane $(r, \theta)$ imposes onto the circulation flow in the plane $(r, z)$. As the jet surface in the region of vortex incipience is convex rather than concave, however, these vortices are not caused by the Taylor–Görtler instability [9]. In contrast to pairs of steady Taylor–Görtler vortices, the single annular vortices formed here are unsteady: they move in the radial direction and, correspondingly, are extended in the tangential direction. The circular (tangential) velocity rapidly decreases with increasing radius and equals zero outside the vortex structure and the jet (Fig. 3b).

It should be noted that the unsteady character of the external flow has almost no effect on the positions of streamlines inside the porous body, which remain unchanged, except for a small region near the side surface in the vicinity of the corner. Thus, the flow inside a rotating porous body remains stable and steady.

**Specific Features of the Flow between a Rotating Porous Disk and a Flat Screen (Problem 2).** Engineering equipment often involves configurations with rotating bodies being placed into various gaps. In the case of rotation of a CPM body under such conditions, the external flow and the gas flow through the porous body are limited by the planes outside the body. This can lead to a cardinal reconstruction of the internal flow and favor the formation of stagnant regions. Therefore, it is of interest to study the specific features of the flow between a rotating porous body and a flat screen.

The experimental studies were performed with a cylindrical porous body; one of its end faces was impermeable (covered by a soldered thin disk). At a certain distance from the other end face, there was a flat screen of circular shape, which limited the air inflow (Fig. 4). The values of $\Delta p_+ = p_+ - p_0$ and $\Delta p_- = p_- - p_0$ were measured by a Pitot tube at points with identical values of $H$ ($H$ is the distance from the screen plane to the measurement point) and $|r_+| = |r_-|$ (Fig. 4). The following parameters were used in solving the problem: disk diameter 150 mm, disk thickness 25 mm, screen diameter 150 mm, distance between the screen and the disk 20 mm,

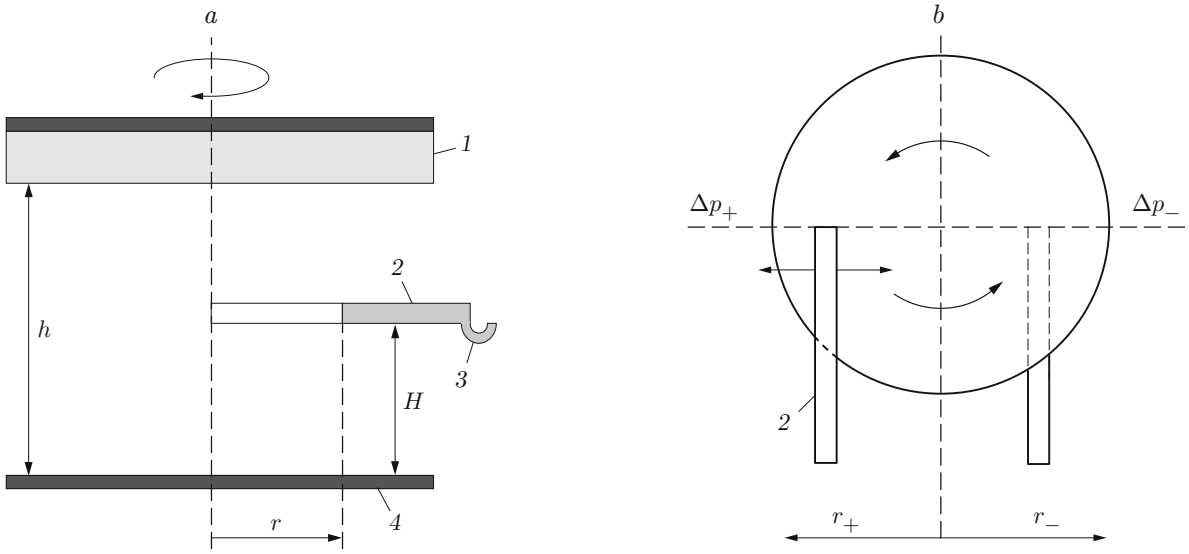


Fig. 4. Sketch of the experimental setup: cross-sectional view (a) and view from the screen (b); 1) disk; 2) probe; 3) U-tube manometer; 4) screen.

TABLE 1

Tangential Velocity $w$ in the Gap between a Cellular-Porous Disk and a Flat Screen

| $r$ | $h = 0$ | | $h = 0.0667$ | | $h = 0.1267$ | | $h = 0.2$ | |
|---|---|---|---|---|---|---|---|---|
| | Exp. | Comput. | Exp. | Comput. | Exp. | Comput. | Exp. | Comput. |
| 1.0 | 0.33 | 0.40 | 0.41 | 0.41 | 0.43 | 0.44 | 0.45 | 0.50 |
| 0.867 | 0.41 | 0.50 | 0.45 | 0.51 | 0.45 | 0.54 | 0.41 | 0.62 |
| 0.733 | 0.43 | 0.60 | 0.48 | 0.61 | 0.48 | 0.62 | 0.45 | 0.65 |
| 0.6 | 0.44 | 0.64 | 0.50 | 0.65 | 0.52 | 0.64 | 0.46 | 0.64 |
| 0.467 | 0.50 | 0.61 | 0.55 | 0.61 | 0.55 | 0.60 | 0.45 | 0.59 |
| 0.333 | 0.18 | 0.53 | 0.53 | 0.53 | 0.49 | 0.53 | 0.32 | 0.51 |
| 0.2 | 0 | 0.46 | 0.39 | 0.46 | 0.36 | 0.46 | 0.13 | 0.42 |
| 0.0667 | 0.13 | 0.16 | 0.22 | 0.16 | 0.26 | 0.16 | −0.13 | 0.14 |

and velocity of disk rotation 2820 rpm. The corresponding dimensionless values of tangential velocity determined by the formula $w = \sqrt{\Delta p/(\rho_0 R^2 \Omega^2)}$, where $\Delta p = \Delta p_+ - \Delta p_-$ and $\rho_0 = 1.2$ kg/m$^3$ (for $p_0 = 1$ atm and $T_0 = 20$ °C), for $R = 0.075$ m and $\Omega = 2820$ rpm are listed in Table 1. The values of $r$ and $h$ are normalized to $R$.

The results of a preliminary analysis of experimental data on tangential velocity of the flow in the gap between a porous body and a flat screen allow us to draw the following conclusions:

1) for $r \leqslant 40$ mm, the tangential velocity in the core flow is distributed in the same manner as that in the solid body; this velocity is slightly higher than the disk velocity;

2) for $r \approx 45$ mm, the tangential velocity is consistent with the disk velocity and remains almost constant for $r > 45$ mm.

The flow was computed within the framework of the model developed in [3]. Equations (1) with appropriate boundary conditions were solved numerically with the use of the same method that was applied in solving Problem 1. To determine the steady flow, we solved a time-dependent problem in the domain $r_{\text{in}} \leqslant r \leqslant r_1$, $0 \leqslant z \leqslant z_1$. The porous body was restricted to the region $r_{\text{in}} \leqslant r \leqslant 1$, $z_1 - z_0 \leqslant z \leqslant z_1$, and the screen occupied some part of the boundary $z = 0$, $r_{\text{in}} \leqslant r \leqslant 1$. Here $r_{\text{in}}$ is the radius of the impermeable axis where the rotating CPM disk is attached (as $r_{\text{in}}$ is a rather small quantity, the computational domain outside the porous disk is also restricted to this value), $z_1$ is the distance between the screen and the closed end face of the disk, and $r_1$ is the radius of the external boundary of the computational domain; the screen and the disk have identical radii. Zero values of all functions were prescribed as the initial conditions.

In accordance with the physical formulation of the problem, the following conditions were set on the input boundary and on the internal axis: $\chi = 0$, $v = 0$, and $\partial w/\partial z = 0$ for $z = 0$ and $r_{\text{in}} \leqslant r \leqslant 1$; $\chi = 0$, $u = 0$, and $\partial v/\partial r = 0$ for $r = r_{\text{in}}$ and $0 \leqslant z \leqslant z_1$; $\partial\chi/\partial z = 0$, $v = 0$, and $\partial w/\partial z = 0$ for $z = z_1$ and $r_{\text{in}} \leqslant r \leqslant 1$; $\chi = 0$, $u = 0$, and $\partial w/\partial z = 0$ for $z = 0$ and $1 < r \leqslant r_1$. Several different variants of "soft" ("extrapolated") boundary conditions were considered. The computations showed that these conditions affect the solution only in a certain vicinity of the upper boundary, whereas the computed patterns of the flow between the porous disk and the screen and inside the porous disk are almost identical.

For $z = 0$ and $r_{\text{in}} \leqslant r \leqslant 1$, the following boundary conditions were set on the screen surface: $\alpha u + (1 - \alpha)\,\partial u/\partial z = 0$, $v = 0$, and $\alpha w + (1 - \alpha)\,\partial w/\partial z = 0$, where $\alpha \in [0, 1]$ is a certain accommodation coefficient. For $\alpha = 1$, these conditions coincide with no-slip conditions for a viscous flow, and the value $\alpha = 0$ corresponds to the condition of an ideally smooth wall. In the general case, the flow with certain slipping is modeled at low values of $\alpha$. Note that the distribution of $w$ over $z$ is close to linear in numerical computations with $\alpha = 1$ in the gap between the rotating porous disk and the flat screen, which contradicts dynamic pressure measurements. The computations reveal the trend to formation of a core flow rotating with a velocity equal to or greater than the velocity of revolution of the solid body, but this trend in computations is rather weak. The domain where $w$ is greater than its value inside the porous body is small, is adjacent to the axis, and has a triangular shape. Thus, modeling of the flow under complete no-slip conditions on the wall does not capture the specific features of experimentally observed characteristics. A possible reason is generation of three-dimensional perturbations by a nonuniform cellular structure of a rapidly rotating porous body in experiments. The flow is unstable to these perturbations, similar to the flows between oppositely rotating planes or between a motionless plane and a rotating plane [10]. Spiral and circular waves being formed [10] lead to near-wall swirl redistribution and formation of a wider (more "filled") velocity profile. An axisymmetric model is obviously unsuitable for a detailed description of such flows, and the full problem has to be solved in a three-dimensional formulation. Nevertheless, some mean axisymmetric flow can be modeled with an accommodation coefficient $\alpha < 1$. In particular, for $\alpha = 0$ used in the present computations, the effect of the boundary layer on the wall is neglected, and viscosity is taken into account only in the internal flow. Apparently, the boundary-layer thickness in a real flow is small.

The computed results are plotted in Fig. 5 (the porous body is shown as a rectangle). A typical pattern of streamlines is shown in Fig. 5a, and the vector field of the radial and longitudinal velocity components is shown in Fig. 5b. A specific feature of the flow formed between the disk and the screen is its separation into two parts. In one part of the flow ($r > 0.5$), the gas enters from the external region, passes through the porous body, and departs back to the external region. In the internal region ($r < 0.5$), the streamlines are closed; they pass both through the porous body and through the region located between the disk and the plane screen. Owing to the weak flow, the zone located below the zero streamline cannot be considered as a stagnant zone: a closed annular vortex is formed here (Fig. 5b). In addition, the flow is also characterized by swirl in the direction of rotation of the porous body; hence, the spatial gas flow involves motion with helical trajectories. A two-dimensional distribution of the tangential component of velocity $w$ is plotted in Fig. 5c. In the steady flow, the values of $w$ in the region between the porous body and the screen are higher than the values inside the porous body, which is also noted in experiments. Apparently, such a distribution is caused by transfer of tangential swirl in the backflow near the porous body. It follows from the analysis of the equation for $w$ of system (1) that the change in $rw$ along the streamline is caused only by viscous terms (in the absence of viscosity along the streamline $rw = \text{const}$; correspondingly, $w$ is proportional to $1/r$). By virtue of this condition, the values of $w$ increase outside the body, in the backflow region (with negative values of $u$) as the radius decreases; the values of $w$ inside the porous body are close to the angular velocity of disk rotation: $w \approx r$. Viscous terms promote smoothing of the distribution of $w$ both over $z$ and, to a certain extent, over $r$. For this reason, the values of $w$ in the gap for small values of $r$ are higher than those inside the porous body; as $r$ increases, the values of $w$ reach a plateau, as is observed in experiments as well. In computations, this domain is bounded by the values $0.45 < r < 0.75$, and an insignificant decrease in $w$ is only observed in computations when approaching the edge of the screen.

The experimental and computed values of $w$ are listed in Table 1. Though the computed tangential velocity of the flow in the gap is slightly higher than the experimental values, the qualitative behavior of the results is fairly consistent. The quantitative difference is caused by the constraints of the numerical model and by a certain scatter of experimental data.

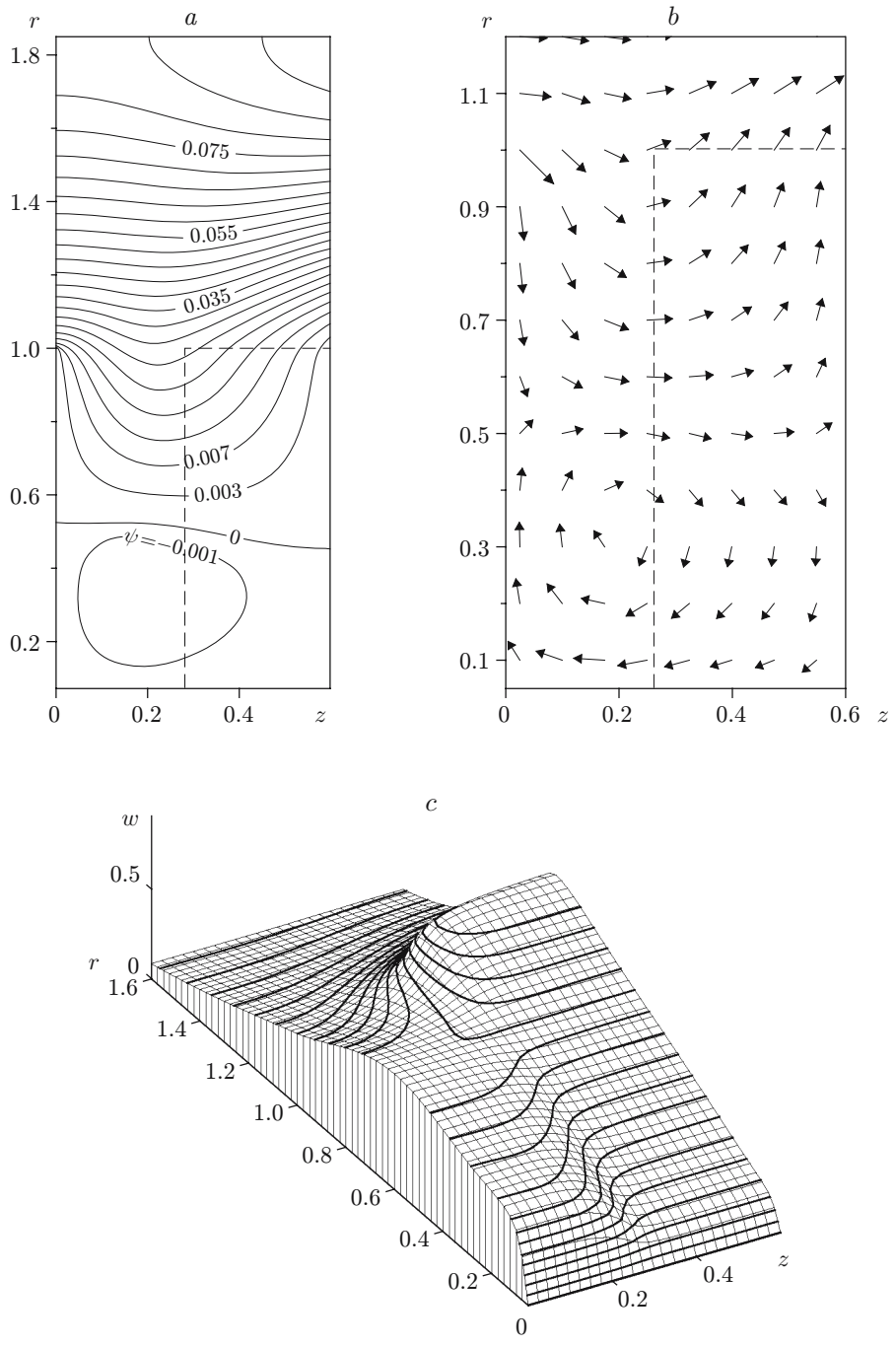


Fig. 5. Characteristics of the flow in the case of rotation of a CPM disk near a flat screen: (a) streamlines; (b) vector flow field; (c) tangential velocity distribution.

**Conclusions.** The flow with a rotating body made of a cellular-porous material is studied numerically and experimentally. The following results are obtained.

The boundaries of stability of the steady flow are determined for a porous disk rotating in free space. It is shown that the external flow loses its stability by the Kelvin–Helmholtz type with increasing Reynolds number, which is manifested in formation of a vortex sheet at the boundary of a swirl jet ejected through the side surface by centrifugal forces. The flow inside the rotating porous body remains stable and steady.

For a CPM disk rotating near a flat screen, the existence of a flow region in the gap with tangential velocity higher than the velocity of rotation of the solid body is demonstrated experimentally and confirmed numerically. The existence of a closed swirl flow, which covers the region inside and outside the porous body and leads to swirl redistribution, is revealed numerically.

This work was partly supported by the Russian Foundation for Basic Research (Grant No. 06-01-00299) and was performed within the Integration Project No. 83 of the Siberian Division of the Russian Academy of Sciences.

## REFERENCES

1. V. K. Baev and V. M. Fomin, "Main ideas of interdisciplinary projects of new types of energy-transducing facilities," in: *Proc. of the Int. Conf. on Methods of Aerodynamic Research* (Novosibirsk, Russia, June 28–July 3, 2004), Part I, Publ. House "Nonparallel," Novosibirsk (2004), pp. 26–29.
2. A. V. Fedorov, V. M. Fomin, and T. A. Khmel', "Mathematical modeling of flows inside rotating bodies made of cellular-porous materials," *J. Appl. Mech. Tech. Phys.*, **46**, No. 6, 835–841 (2005).
3. V. K. Baev, A. V. Fedorov, V. M. Fomin, and T. A. Khmel', "Centrifugal convection in rapid rotation of bodies made of cellular-porous materials," *J. Appl. Mech. Tech. Phys.*, **47**, No. 1, 36–46 (2006).
4. A. M. Beklemyshev, "Specific features of the drag law in high-porous cellular materials," Republican Engineering Center of Powder Metallurgy and Institute of Problems of Powder Technology and Coatings and Pilot Production, Perm' (1996). Deposited at VINITI, 07.09.96, No. 2265-B96.
5. T. A. Pupykina, "Numerical calculation of inviscid MHD flow around complex-shaped bodies," in: *Numerical Methods of Mechanics of Continuous Media* (collected scientific papers) [in Russian], Vol. 16, No. 4, Inst. Theor. Appl. Mech., Sib. Div., Acad of Sci. of the USSR, Novosibirsk (1985), pp. 95–110.
6. P. J. Roache, *Computational Fluid Mechanics*, Hermosa, Albuquerque (1976).
7. M. I. Zhilyaev and T. A. Pupykina, "Modification of a central difference scheme for calculating two-dimensional inviscid flows in force fields," in: *Numerical methods of Mechanics of Continuous Media* (collected scientific papers) [in Russian], Vol. 14, No. 3, Inst. Theor. Appl. Mech., Sib. Div., Acad of Sci. of the USSR (1983), pp. 65–75.
8. L. D. Landau and E. M. Lifshits, *Course of Theoretical Physics*, Vol. 6: *Fluid Mechanics*, Pergamon Press, Oxford-Elmsford, New York (1987).
9. P. M. Eagles, "Taylor–Görtler disturbances in thin film flow: A perturbation method," *Fluid Dyn. Res.*, **15**, 405–423 (1995).
10. L. Schouveiler, P. Le Gal, M. P. Chauve, and Y. Takeda, "Spiral and circular waves in the flow between a rotating and a stationary disk," *Exp. Fluids*, **26**, 179–187 (1999).